Science and Technology for Energy Transition **79**, 68 (2024)

https://doi.org/10.2516/stet/2024066

Decarbonizing Energy Systems: Smart Grid and Renewable Technologies
Fang Rui-ming and Qiangqiang Liao (Guest Editors)

Available online at:
stet-review.org

REGULAR ARTICLE OPEN ACCESS

Day-ahead optimal dispatching for airport-integrated energy system based on load-storage coordination

Yuejie Wang and Ruiming Fang*

College of Information Science and Engineering, Huaqiao University, Xiamen 361021, China

Received: 7 July 2024 / Accepted: 11 August 2024

Abstract. Airports are characterized by high energy consumption, with the cooling supply load being the primary contributor. Optimal dispatching by utilizing the elastic characteristics of cooling supply load is the key to energy saving and decarbonization of airports. Firstly, this paper proposes to build a load-storage integrated energy system architecture by incorporating the ice storage system; secondly, a day-ahead optimal dispatching model to minimize operating costs and carbon emissions is established; finally, taking an airport as the example, the NSGA-II algorithm is applied to solving the model, and the optimal solution for each energy equipment output plan is obtained. The proposed model is compared and analysed under the base scenario, photovoltaic output fluctuation and outdoor temperature variation scenarios, and the daily photovoltaic consumption rate and indoor temperature range are used to evaluate the dispatching results. The optimal dispatching model improves its performance greatly compared to the design condition, with a reduction of 33.3% for the operating cost and 31.9% for the carbon emissions, and the results demonstrate that the proposed model can almost achieve full photovoltaic consumption while ensuring that the indoor temperature is maintained in the passengers' comfort zone in the face of different levels of photovoltaic output fluctuations and outdoor temperatures. Research outcomes in this paper fill the gap in the optimised potential exploitation of cooling supply loads, respond to the dispatching pressure caused by the energy consumption characteristics of airports, and provide a reference for renewable energy access and energy flexibility management in airports.

Keywords: Integrated energy system for airports, Cooling supply load elasticity, Ice storage system, Load-storage coordination, Photovoltaic consumption, Comfort degree.

1 Introduction

As energy-intensive infrastructure, airports require a significant amount of energy consumption for air conditioning, lighting, gates, and other equipment [1, 2]. Airports are also notable sources of carbon dioxide emissions [3], accounting for 0.05% of global energy-related carbon dioxide emissions [4] according to the International Energy Agency. Therefore, optimal dispatching of the Airport Integrated Energy System (AIES) is crucial for achieving dual-carbon goals and is a current research hotspot.

Integrating renewable energy has become the key to energy conservation and carbon emission reduction at airports. The research included in [5] proposed a new microgrid processing scheme for airports by combining solar, hydrogen and energy storage, significantly reducing the annual cost and carbon emissions. The new energy generation proportion in Beijing Daxing International Airport reached 10% [5, 6] established a spatial-temporal passenger distribution model, and the calculated of the HVAC system's energy consumption than the existing model reduced by 11.3%. For the Copenhagen Airport, a method is proposed in [7] to ensure that the photovoltaic panel's reflections do not jeopardize flight safety so that the airport can rely on photovoltaic power generation to meet part of its energy needs. However, as a renewable energy source, the volatility and intermittency of photovoltaic power generation will bring challenges to the safe and stable operation of AIES, and the consumption of renewable energy output is not included in the above studies.

Realizing load flexibility management is significant for improving the airport energy systems efficiency [8]. In AIES, the cooling supply load is a kind of elastic load with a large inertia constant coefficient, which is manifested as the response of the cooling supply system is delayed from the load change, thus buffering the direct impact of the external temperature change on the indoor environment, and reshaping the load curve through the reasonable

* Corresponding author: fangrm@hqu.edu.cn

adjustments can reduce the energy consumption of airports [9]. The cooling supply load occupies a large proportion of the energy system of airports, especially in the southern regions, the demand for cooling supply load in summer accounts for 80-85% of the total cooling energy load [10], presenting significant potential for efficiency optimization. The studies in [11] proposed a near-zero-energy airport concept for the airport's central air-conditioning system, which maximizes the energy utilization of the airport by adjusting the fluid temperature in the cooling grid. Prasetyo *et al.* [12] and Arifin *et al.* [13] conducted research through computational fluid dynamics modelling and solar radiation intensity change simulation respectively, and the results proved that the optimisation of the fluid parameters in the cooling grid can improve the electric conversion efficiency of photovoltaic panels. The above studies further demonstrate the feasibility of optimizing the cooling grid to enhance energy efficiency in AIES with high photovoltaic integration.

Maintaining indoor temperature to ensure passenger comfort is crucial in airport energy application and management [7]. Integrating Ice Storage System (ISS) to improve the flexibility of the cooling system has become an important way to achieve load-storage coordination in AIES. Grid stability is achieved by controlling the ice storage/melting decisions of the Ice Storage Device (ISD) in the ISS [14]. Shi *et al.* [15] analyzed the performance of the ISS in an international airport and found that integrating ISS reduces annual operating costs by 51.3%. By improving the building information modelling platform, Kurniawan *et al.* [16] can obtain accurate optimisation objective values of the studied buildings, and the research provides an effective means for aggregating optimization techniques in large building models. Facing AIES with extremely high energy consumption, how to satisfy the system energy supply requirements through dispatching while guaranteeing safe and stable operation is the main challenge in day-ahead dispatching [8]. Studies on optimal load-storage coordination in AIES for hot and humid climates are limited, especially regarding ISS characteristics, photovoltaic consumption, and passenger comfort, with insufficient focus on cooling supply loads.

This paper firstly constructs the AIES architecture including ISS; then, combining the "high generation and low storage" characteristics of the ISS and cooling supply load elasticity, a day-ahead optimal dispatching model of AIES based on load-storage coordination was proposed to cope with the high energy consumption and strict indoor environmental control requirements in the hot and humid southern region; finally, the NSGA-II algorithm is used to optimizes the balance between economic and environmental benefits. A large international airport in southern China is taken as an example to verify the proposed model's effectiveness.

The subsequent sections of the manuscript are organized as follows: Section 2 models the constructed AIES and its internal units. Section 3 models the day-ahead optimal dispatching based on cooling supply load elasticity. Section 4 analyzes the obtained results by setting up different scenarios. Section 5 concludes the paper.

2 Integrated energy system architecture for the airport incorporating ice storage system

The AIES with ISS as a load-storage coordination module is shown in Figure 1. The source side includes the power grid, gas grid and Photovoltaic (PV) [17]. Multiple energy sources are coupled *via* the Combined Cooling Heating and Power (CCHP) unit, which includes an Absorption Chiller (AC), gas turbine, gas boiler and waste heat boiler. The load-side comprises electric, heat, and cooling loads, with cooling loads divided into rigid (e.g., navigation systems) and elastic (e.g., cooling supply loads with high inertia) [18]. Demand response is considered on the electric load side. The storage side mainly includes ISS.

2.1 Ice storage system modelling

In the hot southern climate, especially during summer, airports have a high cooling supply demand. Thus, ISS is integrated into the AIES to coordinate load and storage for efficient operation. ISS consists of Electric Chiller (EC), AC, ISD and auxiliary equipment [19]. It stores ice during low electricity price periods and melts it during peak demand or high price periods. ISD operates in two modes: ice storage charging and ice melting discharging, as defined by equations (1) and (2) [20]:

$$\begin{cases} E_{\text{ice}}^{24} = E_{\text{ice}}^{0} \\ E_{\text{ice}}^{\min} \le E_{\text{ice}}^{t} \le E_{\text{ice}}^{\max} \\ E_{\text{ice}}^{t+1} = E_{\text{ice}}^{t}(1-\delta_{\text{ice}}) + \left(P_{\text{ice},c}^{t}\eta_{\text{ice},c} - \frac{P_{\text{ice},d}^{t}}{\eta_{\text{ice},d}}\right)\Delta t \end{cases}, \tag{1}$$

$$\begin{cases} 0 \le P_{\text{ice},c}(t) \le \mathrm{u}_{\text{ice}} \cdot P_{\text{ice},c}^{\max} \\ 0 \le P_{\text{ice},d}(t) \le (1-u_{\text{ice}}) \cdot P_{\text{ice},d}^{\max} \\ P_{\text{ice},c}(t) = a_c + b_c Q_{\text{ice},c}(t) + c_c Q_{\text{ice},c}^{2}(t) + d_c Q_{\text{ice},c}^{3}(t) \\ P_{\text{ice},d}(t) = a_d + b_d Q_{\text{ice},d}(t) + c_d Q_{\text{ice},d}^{2}(t) + d_d Q_{\text{ice},d}^{3}(t) \end{cases}, \tag{2}$$

where: δ_{ice} is the ISD loss limit; u_{ice} is a 0-1 variable; $P_{\text{ice},c}(t)$ and $P_{\text{ice},d}(t)$ are the ISD charge/discharge power at hour t; $P_{\text{ice},c}^{\max}$ and $P_{\text{ice,d}}^{\max}$ are ISD maximum charge/discharge power; E_{ice}^{t+1} and E_{ice}^{t} are the stored energy after/before the mode conversion; $E_{\text{ice}}^{\min}$ and $E_{\text{ice}}^{\max}$ are the lower/upper limit of the stored energy of the ISD; $Q_{\text{ice},c}(t)$ and $Q_{\text{ice},d}(t)$ are the charge/discharge capacity of the ISD at hour t; a_c, b_c, c_c, d_c, a_d, b_d, c_d, d_d are regression coefficients.

2.2 Renewable energy modelling

The Beta distribution is used to simulate the solar irradiation intensity of the day to build the PV output model [21], as shown in equations (3) and (4):

$$P_{\text{PV}}(t) = S(t)A\eta, \tag{3}$$

$$f(S) = \frac{\Gamma(\alpha+\beta)}{\Gamma(\alpha)\Gamma(\beta)} \cdot \left(\frac{S}{S_{\max}}\right)^{\alpha-1} \cdot \left(1-\frac{S}{S_{\max}}\right)^{\beta-1}, \tag{4}$$

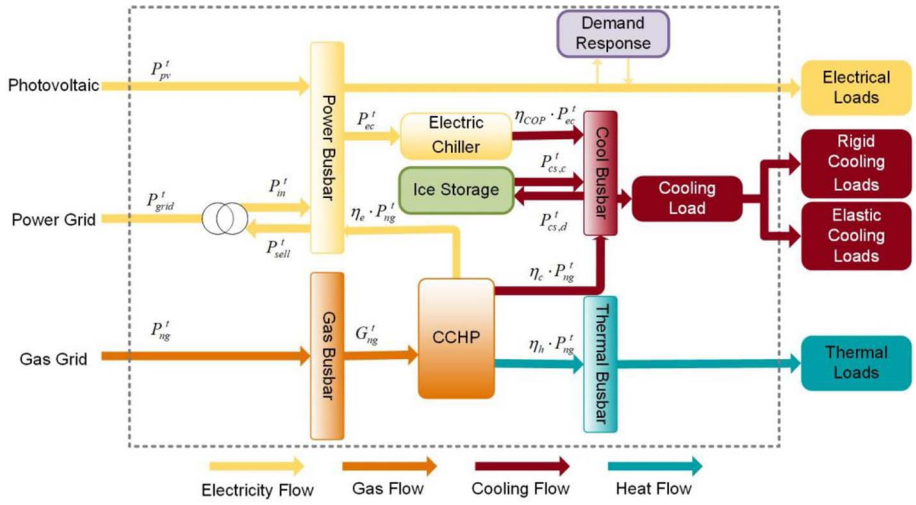

Fig. 1. Integrated energy system architecture for airport.

where: $P_{\mathrm{PV}}(t)$ is the output power of the PV panels at hour t; A is the PV array area; η is the photoelectric conversion efficiency. $f(S)$ is the probability density function of the Beta distribution; $\Gamma(\cdot)$ is the gamma function; S and $S_{\max}$ are the actual and the maximum irradiation intensity; α and β are the shape parameters.

2.3 CCHP unit modelling

The model of CCHP is shown in equation (5).

$$\begin{cases} P_c(t) = \eta_c P_{\mathrm{ng}}(t) \\ P_e(t) = \eta_e P_{\mathrm{ng}}(t) \\ P_h(t) = \eta_h P_{\mathrm{ng}}(t) \end{cases} \tag{5}$$

where: $P_c(t)$, $P_e(t)$ and $P_h(t)$ are the cooling, electric and thermal output power of the CCHP at hour t; $P_{\mathrm{ng}}(t)$ is the natural gas input power at hour t; η_c, η_e and η_h are the cooling, electric and thermal efficiency [22] of the CCHP.

2.4 Cooling supply load elasticity analysis

During the cooling process, the temperature change of the chilled medium usually lags behind that of the cooling medium, maintaining room comfort for a period after cooling stops [23]. In addition, passengers' temperature perception is elastic [24], allowing minor changes in cooling temperature without affecting comfort. Based on the above characteristics, utilizing Cooling Supply Load Elasticity (CSLE) characteristics can improve AIES operating economy. Accordingly, the Predicted Mean Vote (PMV) index was introduced to evaluate the indoor temperature comfort level to quantify the comfort level of passengers in the system. The PMV is based on the ASHRAE Thermal Awareness Scale for predicting the average response of a population [25], and is calculated as equation (6) after a simplified engineering treatment:

$$\lambda_{\mathrm{PMV}} = 2.43 - \frac{3.76(t_s - t_a)}{MR(I_{\mathrm{cl}} + 0.1)}, \tag{6}$$

where: MR is the human metabolic rate; I_{cl} is the thermal resistance of clothing; t_s is the average human skin; and t_a is the air temperature around the body.

The PMV index corresponds to the seven thermal sensations of the human body on a 7-level scale, and the PMV value of 0 corresponds to the optimal thermal comfort state of the human body [26]. Daytime demands higher comfort due to frequent passenger activity, while nighttime allows for relaxed comfort standards. Accordingly, the time-sharing limit of PMV is set, as shown in Figure 2.

3 Day-ahead optimal dispatching model for integrated energy system at airport considering CSLE

3.1 Objective function

Day-ahead optimal dispatching model takes the lowest operating cost and the smallest environmental cost as the optimal dispatching objectives.

3.1.1 Operating cost

The minimum operating cost is shown in equations (7) and (8), including the purchase and sale cost $C_{\mathrm{grid}}(t)$, the penalty cost for solar curtailment $C_{\mathrm{loss}}(t)$, the maintenance cost $C_m(t)$, and the revenue from electricity sales $C_{\mathrm{sell}}(t)$:

$$\min f_1(t) = \sum_{t=1}^{T} \left(C_{\mathrm{grid}}(t) + C_{\mathrm{loss}}(t) + C_{\mathrm{m}}(t) - C_{\mathrm{sell}}(t) \right), \tag{7}$$

$$\begin{cases} C_{\mathrm{grid}}(t) = \sum_{t=1}^{24} C_{\mathrm{e}}(t) P_{\mathrm{in}}(t) + \sum_{t=1}^{24} C_{\mathrm{g}}(t) P_{\mathrm{ng}}(t) \\ C_{\mathrm{m}}(t) = \sum_{t=1}^{n} k_i P_i(t) \\ C_{\mathrm{sell}}(t) = C_{\mathrm{e}}(t) \sum_{t=1}^{24} \Delta t P_{\mathrm{out}}(t) \end{cases}, \tag{8}$$

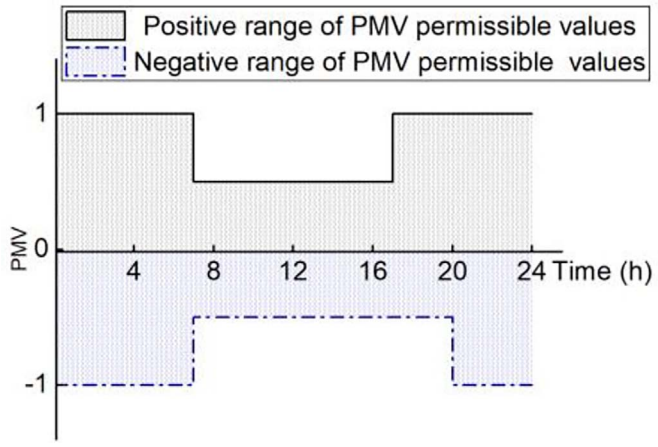

Fig. 2. Regulatory range of PMV values.

where: T is the total dispatching periods; C_e and C_g are the electricity and natural gas prices; $P_{\text{in}}(t)$ is the power input at hour t; k_i and $P_i(t)$ are the unit maintenance cost and output power of each device at hour t; and $P_{\text{out}}(t)$ is the active power sold to the grid at hour t.

The $C_{\text{loss}}(t)$ is caused by the phenomenon of failing to fully utilize PV, for which the segmentation penalty coefficient $g_p(t)$ is introduced [27] in equation (9):

$$\begin{cases} C_{\text{loss}} = \sum_{t=1}^{24} g_p(t) C_e(t) A_{\text{PV}}(t) \\ g_p(t) = \begin{cases} 1.25 & \pi_{PV}^t > 3\% \\ 0.75 & 0 \le \pi_{PV}^t \le 3\% \end{cases} \end{cases}, \tag{9}$$

where: A_{PV} (t) is the discarded power at hour t; π_{PV}^t is the discard rate at hour t.

3.1.2 Environmental cost

Environmental costs consist primarily of emissions from grid interactions [28], as shown in equation (10):

$$\min f_2(t) = \sum_{i=1}^{\text{T}} \mu_e P_{\text{grid}}(t), \tag{10}$$

where: $A_{\text{PV}}(t)$ is the discarded power at hour t; π_{PV}^t is the discard rate at hour t.

3.2 Optimizing variable

The output plan of each energy equipment is selected as the optimal dispatching variable. To highlight the influence of CSLE and due to its high proportion in the overall cooling load, the cooling supply load is mainly considered in the analysis. In the conventional cooling grid, the power balance of the cooling system is equationally constrained, as shown in equation (11).

$$P_c(t) + C_{\text{EC}}(t) + P_{\text{ice},d}(t) - P_{\text{ice},c}(t) = L_C(t), \tag{11}$$

where: $C_{\text{EC}}(t)$ is the output power of the EC at hour t; $L_C(t)$ is the cooling supply load of the system at hour t.

After considering CSLE, the cooling capacity is transformed from a fixed value to an interval value, as shown in equation (12).

$$\begin{cases} L_C(t)_{\min} \le P_c(t) + C_{\text{EC}}(t) + P_{\text{ice},d}(t) - P_{\text{ice},c}(t) \le L_C(t)_{\max} \\ \begin{cases} L_C(t)_{\min} = (1 - k_{\text{down}}) L_C(t) \\ L_C(t)_{\max} = (1 + k_{\text{up}}) L_C(t) \end{cases} \end{cases}, \tag{12}$$

where: $L_C(t)_{\min}$ and $L_C(t)_{\max}$ are the lower/upper limit of the cooling supply load value under the premise of meeting the comfort level of passengers; k_{down} and k_{up} are the elasticity coefficients of the cooling supply loads.

3.3 Constraint condition

3.3.1 Solar curtailment power constraints

$$\sum_{t=1}^{T} P_{\text{PV}}(t) - \sum_{t=1}^{T} P_{\text{PV}}^{\min}(t) \le \pi_{\text{PV}}^{\max} \sum_{t=1}^{T} P_{\text{PV}}(t), \tag{13}$$

where: $P_{\text{PV}}^{\min}(t)$ is the minimum acceptable PV output power at hour t; $\pi_{\text{PV}}^{\max}$ is the maximum allowable solar curtailment ratio.

3.3.2 ISS operational constraints

$$\begin{cases} P_{\text{EC}}(\text{t}) \text{COP}_{\text{EC}} = C_{\text{EC}}(t) \\ P_{\text{WHB}}(t) \text{COP}_{\text{AC}} = C_{\text{AC}}(t) \end{cases}, \tag{14}$$

where: $P_{\text{EC}}(t)$ is the input power of EC at hour t; $P_{\text{WHB}}(t)$ is the output power of the waste heat boiler in CCHP at hour t; COP_{EC} and COP_{AC} are the performance coefficients of EC and AC; $\text{C}_{\text{AC}}(t)$ is the output power of AC at hour t.

The ISD is an important device for the ISS to realize the load-storage coordination and needs to satisfy the constraints shown in equation (15):

$$S_{\text{ice}}(t) = S_{\text{ice}}(t-1) \cdot (1 - \gamma_Q) + \left(\eta_{\text{ice,c}} Q_c(t) - \frac{Q_d(t)}{\eta_{\text{ice,d}}} \right), \tag{15}$$

where: $S_{\text{ice}}(t)$ is the ISD cool energy stored in the ISD at hour t; γ_Q is the self-loss coefficient; $\eta_{\text{ice},c}$ and $\eta_{\text{ice},d}$ are the efficiency coefficients of ice storage and melting.

3.3.3 Power balance of the electrical system

$$\begin{aligned} P_{\text{in}}(t) + P_e(t) + P_{\text{PV}}(t) + \text{DR}(t) \\ = L_E(t) + P_{\text{EC}}(t) + P_{\text{Loss}}(t) \\ P_{\text{grid}}(t) \eta_l = P_{\text{in}}(t), \end{aligned} \tag{16}$$

where: $\text{DR}(t)$ is the change in electrical load after demand response; $P_{\text{Loss}}(t)$ is the electrical loss at hour t; η_t is the transformer efficiency; P_{grid} is the electricity interacting with the grid.

3.3.4 Power balance of the natural gas system in CCHP

$$P_{\text{ng}}(t) = G_{\text{GT}}(t) + G_{\text{GB}}(t), \tag{17}$$

Table 1. System cost parameters.

Type	Parameter	Value
Unit maintenance cost of equipment/(CNY·kW^{-1})	Photovoltaic unit	0.102
	Cold storage unit	0.035
	Gas turbine	0.08
	Waste heat boiler	0.004
	Absorption chiller	0.01
	Gas boiler	0.004
	Electric chiller	0.009
Unit cost of energy/(CNY·kW h^{-1})	Power grid	0.57–1.33
	Gas grid	0.35
CO_2 emission factor/kg·kW h^{-1})	Power grid	0.972
	Gas grid	0.23

Table 2. Ice storage system parameters.

Parameter	Value	Parameter	Value	Parameter	Value
$P_{\text{ice,c}}^{\max}$	3080 kW	$Q_{\text{ice},c}^{\max}$	2800 kW	b_c	1.105
$P_{\text{ice,d}}^{\max}$	3520 kW	$Q_{\text{ice},c}^{\min}$	400 kW	c_c	−1.772e–3
$E_{\text{ice}}^{\max}$	7920 kW h	$Q_{\text{ice},d}^{\max}$	4800 kW	d_c	11.252e–6
$E_{\text{ice}}^{\min}$	1760 kW h	$Q_{\text{ice},d}^{\min}$	400 kW	a_d	−2.256
$\eta_{\text{ice},c}$	0.97	COP_{EC}	4	b_d	0.71
$\eta_{\text{ice},d}$	0.95	COP_{AC}	3.5	c_d	5.485e–5
δ_{ice}	0.02	a_c	42.999	d_d	−4.872e–8

where: $G_{\text{GT}}(t)$ and $G_{\text{GB}}(t)$ are the gas consumption power of the gas turbine and gas boiler in the CCHP unit at hour t respectively.

3.3.5 Power balance of the heating system

$$P_h(t) = L_H(t), \tag{18}$$

where: $L_H(t)$ is the heat load of the system at hour t.

3.3.6 Power balance of the cooling system

As described by equation (12).

3.4 Model solution

The NSGA-II algorithm is used to solve the AIES day-ahead optimal dispatching model proposed in this paper. In the process of genetic evolution, the NSGA-II algorithm takes the initial feasible solution of population size as the starting point [29] and selects the compromise optimal solution by plotting the Pareto front [30].

4 Case analysis

The dispatching period is 24 h with a 1-hour step size. The system cost parameters and ISS parameters are listed in Tables 1 and 2. The system load prediction and outdoor temperature for a typical day in summer are shown in Figure 3, indicating the cooling supply load at 45.88% of the total energy demand. The real-time electricity price [31] trend and daily PV forecast curve are shown in Figure 4. Electricity is sold at a constant price of 0.39 CNY/kWh.

4.1 Optimization results

The set of Pareto solutions and optimal compromise solutions are shown in Figure 5. When carbon emissions fall below 15,700 kg, operating costs increase significantly for the same carbon reduction. Therefore, based on the Pareto front congestion degree [32], the optimal compromise solution is selected with equal weights for operating and environmental costs.

The total system cost comparison is shown in Table 3, and the cooling grid dispatching balance results are shown in Figure 6. ISS participates in charges ice with maximum power at the storage-side during low cooling load and low electricity price periods; ISS melts ice and discharges energy with the maximum power in order to satisfy the demand of load-side cool energy during the period of 11:00–13:00 when both the cooling supply load and electricity price are in the peak periods.

4.2 Analysis of PV consumption in different scenarios

The model proposed in equation (4) is used to obtain PV output predictions of different fluctuation degrees based

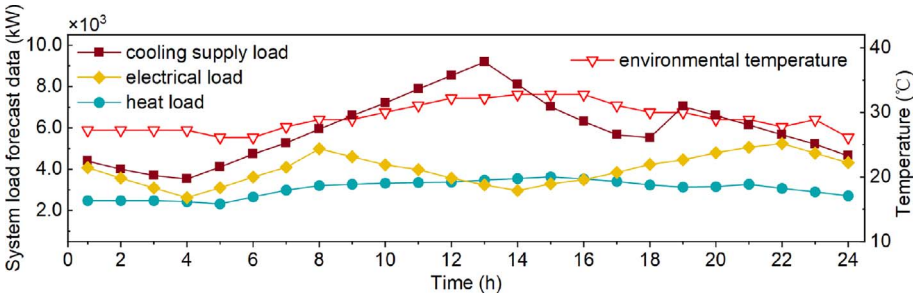

Fig. 3. AIES load forecast curves and outdoor temperatures.

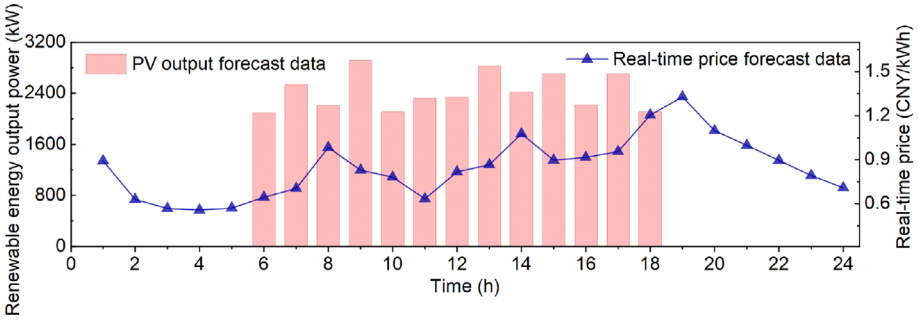

Fig. 4. Real-time price trend and PV output forecast curves.

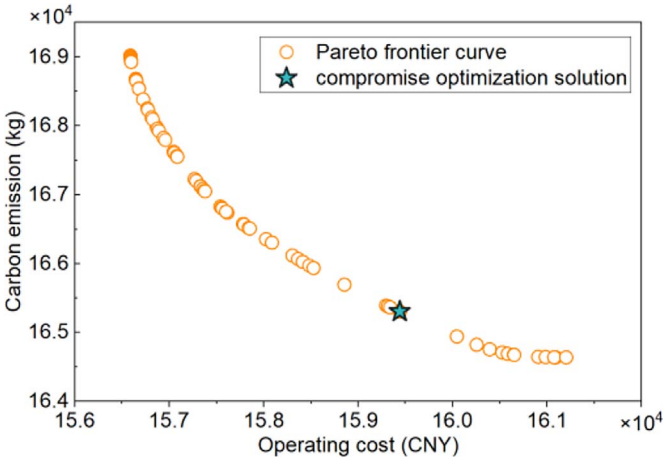

Fig. 5. Distribution of pareto solution set and optimal solution.

on the predicted PV output of typical summer day by changing the standard deviation of the Beta distribution.

Scenario 1: Base scenario.
Typical summer outdoor temperature data and PV output forecast data were used.

Scenario 2: Large fluctuation scenario.
Rapidly changing weather conditions are simulated by amplifying the standard deviation to 2σ.

Scenario 3: Small fluctuation scenario.
Stable weather conditions are simulated by narrowing the standard deviation to 0.5σ.

Table 3. Optimal dispatching results considering CSLE.

Dispatching method	Operating cost /CNY	Environmental costs (carbon emissions)/kg
Routine dispatching	198730.4762	196875.6463
Consider CSLE	165302.841	159440.174

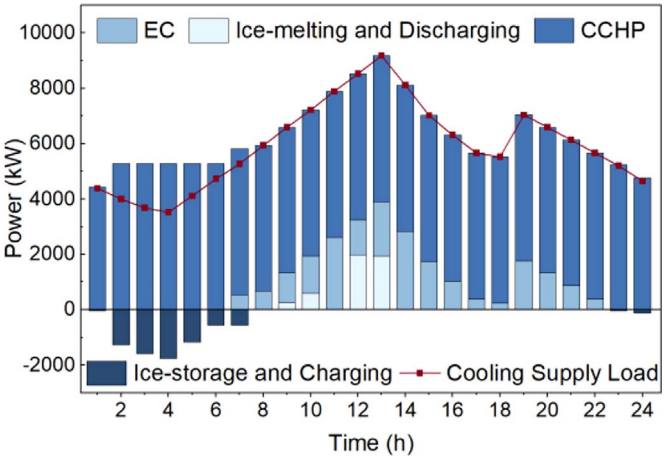

Fig. 6. Power balance of the cooling system.

The total PV output, the PV power for each scenario, and the operating mode and output of the ISS are shown in Figures 7 and 8. During peak cooling load from 10:00 to 13:00 (see Fig. 3), ISS operates in the ice-melting and

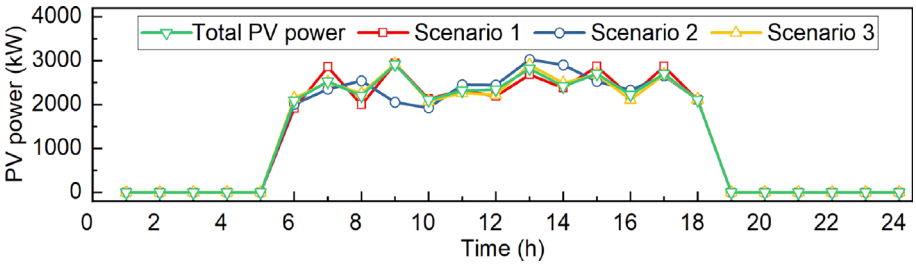

Fig. 7. Total PV power and power of PV output under Scenarios 1, 2 and 3.

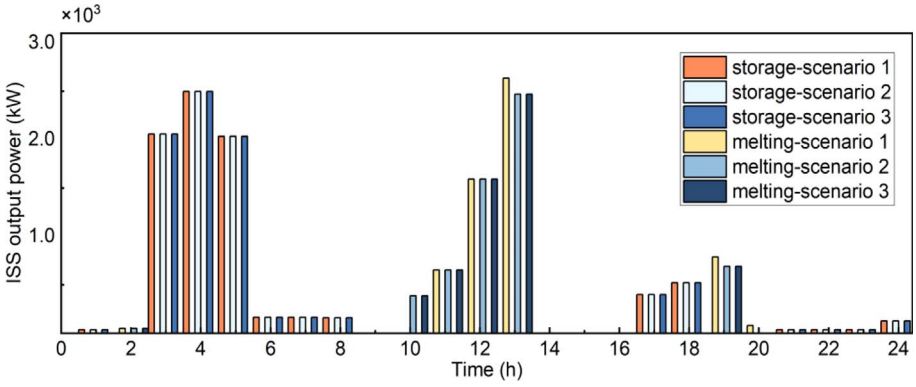

Fig. 8. ISS output power under Scenarios 1, 2 and 3.

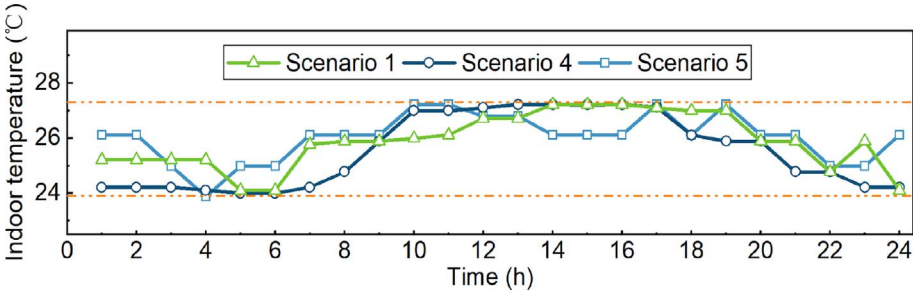

Fig. 9. Indoor cooling temperature under Scenarios 1, 4, and 5.

discharging mode to respond to the load-side cooling supply load. During low cooling load periods from 3:00–8:00 and 17:00–18:00, ISS operates in ice-storage and charging mode to reduce system costs and to realize the adjustment function of the integrated charge-storage module.

After integrating the ISS with dispatching, the daily PV consumption ratios of Scenario 1, Scenario 2, and Scenario 3 are 99.87%, 99.59%, and 99.73% respectively, which basically realize the full consumption of PV output.

4.3 Analysis of passenger comfort in different scenarios

In summer, the indoor temperature comfort range of the airport is 23.9–27.3 °C [33]. Based on scenario 1, the mean daily temperature (average of the highest/lowest temperatures of the day) is selected to characterize the environmental temperature.

Scenario 4: High temperature scenario.

Select the mean daily temperature of 34.45 °C, simulating hot weather conditions.

Scenario 5: Low-temperature scenario.

Select the mean daily temperature of 24.72 °C, simulating relatively cool weather conditions.

Figure 9 shows indoor cooling temperatures for each scenario, with the comfort zone marked by orange dotted lines. All three scenarios maintain temperatures within this zone. Scenario 1 is used for specific analysis.

The cooling supply load changes before and after considering CSLE are shown in equation (12), with corresponding indoor temperature and PMV value changes in Figure 10. The daytime indoor temperature of the airport ranges from 24.1 °C to 27.2 °C, with PMV values from −0.11 to 0.92; after the 21st hour, the PMV value shows a fluctuating

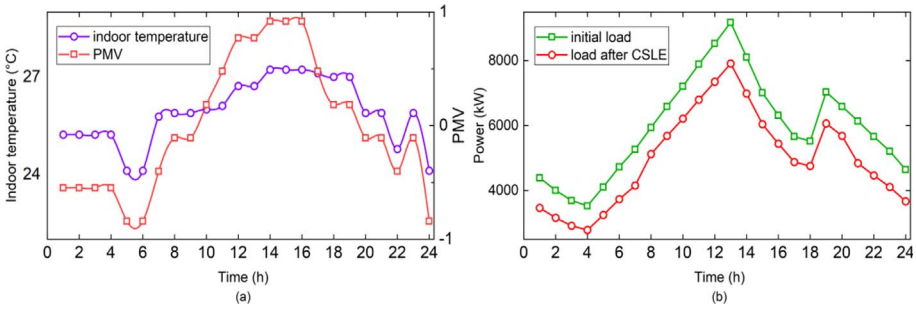

Fig. 10. Scenario 1: a) PMV and indoor temperature curves, b) cooling supply load curves.

tendency of decreasing, then increasing, then decreasing, with the variation range of −0.11 to −0.84, corresponding to the indoor temperature variation range of 24.1–25.8 °C. These results indicate that after considering CSLE, a larger PMV value is selected to ensure higher comfort during the daytime when passenger activities are frequent; at night, the passengers are not sensitive to the perception of temperature at this time, so the PMV value is mostly negative. The airport's cooling supply load curve is optimized by moderately adjusting the PMV value while ensuring indoor cooling comfort.

5 Conclusion

This paper integrates ISS into the AIES as a charge-storage module, combining with CSLE for day-ahead optimal dispatching based on load-storage coordination.

1. Integrating ISS into the system as a load-storage coordination module, and constructing an integrated energy system architecture suitable for large-scale international airports in the southern region by combining the rapid switching process of ISD's working mode with the elastic characteristics of the cooling supply load.
2. The high proportion of cooling supply loads and their elasticity are considered, introducing the PMV index to quantify passenger comfort, and establishing a load-storage coordination day-ahead optimal dispatching model. Compared with routine dispatching, the proposed model reduces the operating cost and carbon emission of the system by 16.8% and 19.0%.
3. By setting up different scenarios for comparison and validation, the proposed model can achieve the full consumption of photovoltaic while ensuring that the indoor cooling temperature is within the passenger's comfort temperature range, provided that the system supply requirements are met. The results demonstrate the feasibility and effectiveness of the proposed model.

The objective functions and optimization approaches used for the model proposed in this paper will be refined in the future to enhance the optimization effect.

Acknowledgments

This work was supported by the Natural Science Foundation of Xiamen (3502Z202373052).

References

1 Zhou Y., Cao S., Kosonen R., Hamdy M. (2020) Multi-objective optimisation of an interactive buildings-vehicles energy sharing network with high energy flexibility using the Pareto archive NSGA-II algorithm, *Energy Convers. Manage.* **218**, 113017.
2 Alba S.O., Manana M. (2016) New Energy research findings reported from University of Cantabria (energy research in airports: a review), *Energy Weekly News* 384.
3 Goh H.H., Suo W., Liang X., Zhang D., Dai W., Kurniawan T. A., Goh K.C. (2024) An adaptive energy management strategy for airports to achieve carbon neutrality by 2050 *via* waste, wind, and solar power, *Front. Energy Res.* **12**, 1365650.
4 Baxter G. (2021) Achieving carbon neutral airport operations by 2025: The case of Sydney Airport, Australia, *Transp. Telecommun. J.* **22**, 1, 1–14.
5 Xiang Y., Cai H., Liu J., Zhang X. (2021) Techno-economic design of energy systems for airport electrification: A hydrogen-solar-storage integrated microgrid solution, *Appl. Energy* **283**, 116374.
6 Gu X., Xie J., Huang C., Ma K., Liu J. (2022) Prediction of the spatiotemporal passenger distribution of a large airport terminal and its impact on energy simulation, *Sustain. Cities. Soc.* **78**, 103619.
7 Baxter G., Srisaeng P., Wild G. (2018) An assessment of airport sustainability, part 2 – energy management at Copenhagen Airport, *Resources* **7**, 2, 32.
8 Jensen S.Ø., Marszal-Pomianowska A., Lollini R., Pasut W., Knotzer A., Engelmann P., Stafford A., Reynders G. (2017) IEA EBC annex 67 energy flexible buildings, *Energy Buildings* **155**, 25–34.
9 Yan C., Wang F., Pan Y., Shan K., Kosonen R. (2020) A multi-timescale cold storage system within energy flexible buildings for power balance management of smart grids, *Renew. Energy* **161**, 626–634.
10 Shaikh Z., Chaudhry H.N. (2018) Energy modelling and indoor air quality analysis of cooling systems for buildings in hot climates, *Fluids* **3**, 4, 77.
11 Kılkış B., Kılkış Ş. (2017) New exergy metrics for energy, environment, and economy nexus and optimum design model for nearly-zero exergy airport (nZEXAP) systems, *Energy* **140**, 1329–1349.
12 Prasetyo S.D., Budiana E.P., Prabowo A.R., Arifin Z. (2023) Modeling finned thermal collector construction nanofluid-based Al_2O_3 to enhance photovoltaic performance, *Civ. Eng. J.* **9**, 12, 2989–3007.
13 Arifin Z., Khairunisa N., Kristiawan B., Prasetyo S.D., Bangun W.B. (2023) Performance analysis of nanofluid-based

photovoltaic thermal collector with different convection cooling flow, *Civ. Eng. J.* **9**, 8, 1922–1935.
14 Brok N., Green T., Heerup C., Oren S.S., Madsen H. (2022) Optimal operation of an ice-tank for a supermarket refrigeration system, *Control Eng, Pract.* **119**, 104973.
15 Shi J., Guo H., Chang C., Dong Z., Shao S., Zheng Z. (2020) Design and Performance Analysis of the Water Cold Storage System in the Energy Center of Pudong International Airport, *Fluid Machinery* **48**, 9, 71–76.
16 Kurniawan T.B., Dewi D.A., Usman F., Fadly F. (2023) Towards energy analysis and efficiency for sustainable buildings, *Emerg. Sci. J.* **7**, 6, 2226–2238.
17 Jiang M., Qi L., Yu Z., Wu D., Si P., Li P., Wei W., Yu X., Yan J. (2021) National level assessment of using existing airport infrastructures for photovoltaic deployment, *Appl. Energy* **298**, 117195.
18 Lin L., Chen G., Liu X., Liu X., Zhang T. (2023) Characterizing cooling load in multi-area airport terminal buildings: Clustering and uncertainty analysis for energy flexibility, *J. Build. Eng.* **79**, 107797.
19 Zhang W., Yu J., Zhao A., Zhou X. (2021) Predictive model of cooling load for ice storage air-conditioning system by using GBDT, *Energy Rep.* **7**, 1588–1597.
20 Heidari A., Mortazavi S.S., Bansal R.C. (2020) Stochastic effects of ice storage on improvement of an energy hub optimal operation including demand response and renewable energies, *Appl. Energy* **261**, 114393.
21 Li S., Gong W., Gu Q. (2021) A comprehensive survey on meta-heuristic algorithms for parameter extraction of photovoltaic models, *Renew. Sustain. Energy Rev.* **141**, 110828.
22 Zhang Y., Si P., Feng Y., Rong X., Wang X., Zhang Y. (2017) Operation strategy optimization of BCHP system with thermal energy storage: A case study for airport terminal in Qingdao, *China, Energy Build.* **154**, 465–478.
23 Zhou C., Jia H., Jin X., Mu Y., Yu X., Xu X., Li B., Sun W. (2023) Two-stage robust optimization for space heating loads of buildings in integrated community energy systems, *Appl. Energy* **331**, 120451.
24 Kotopouleas A., Nikolopoulou M. (2018) Evaluation of comfort conditions in airport terminal buildings, *Build. Environ.* **130**, 162–178.
25 Xiao T., You F. (2024) Physically consistent deep learning-based day-ahead energy dispatching and thermal comfort control for grid-interactive communities, *Appl. Energy* **353**, 122133.
26 Liu X., Lin L., Liu X., Zhang T., Rong X., Yang L., Xiong D. (2018) Evaluation of air infiltration in a hub airport terminal: On-site measurement and numerical simulation, *Build. Environ.* **143**, 163–177.
27 Zhang M., Xu W., Zhao W. (2023) Combined optimal dispatching of wind-light-fire-storage considering electricity price response and uncertainty of wind and photovoltaic power, *Energy Rep.* **9**, 790–798.
28 Ruiming F. (2019) Multi-objective optimized operation of integrated energy system with hydrogen storage, *Int. J. Hydrogen Energy* **44**, 56, 29409–29417.
29 Cococcioni M., Fiaschi L. (2021) The Big-M method with the numerical infinite M, *Optim. Lett.* **15**, 7, 2455–2468.
30 Tavakkoli M., Dehkordi S.F., Kasmaei M.P., Hatziargyriou N., Liski M., Lehtonen M. (2022) Investigating How the Equilibria of the Electricity Market Are Affected by Modeling the strategic Behavior of Consumers, *Int. Rev. Electr. Eng-I.* **17**, 3, 225–247.
31 Yao W., Wang C., Yang M., Wang K., Dong X., Zhang Z. (2023) A tri-layer decision-making framework for IES considering the interaction of integrated demand response and multi-energy market clearing, *Appl. Energy* **342**, 121196.
32 Li L.L., Miao Y., Lim M.K., Sethanan K., Tseng M.L. (2024) Integrated energy system for low-carbon economic operation optimization: Pareto compromise programming and master-slave game, *Renew. Energy* **222**, 119946.
33 Liu J., Yu N., Lei B., Rong X., Yang L. (2009) Research on indoor environment for the terminal 1 of Chengdu Shuangliu international airport, in: J. Zeng (ed.), *Proc. Eleventh International IBPSA conference, Build. Simul., Glasgow, Scotland*, pp. 2138–2145.